Hindawi
Shock and Vibration
Volume 2024, Article ID 8387179, 16 pages
https://doi.org/10.1155/2024/8387179

*Research Article*

# Multiobjective Optimization of Composite Material Seat Plate for Mortar Based on the Hybrid Surrogate Model

**Fengfeng Wang,[1,2] Chundong Xu ,[2] and Lei Li[2]**

[1]*School of Mechanical and Electrical Engineering, Jinling Institute of Technology, Nanjing 211169, China*
[2]*School of Mechanical Engineering, Nanjing University of Science and Technology, Nanjing 210094, China*

Correspondence should be addressed to Chundong Xu; chundongxu@126.com

Received 11 December 2023; Revised 6 January 2024; Accepted 11 January 2024; Published 30 January 2024

Academic Editor: Andrzej Katunin



As an important force transmission component of mortars, the seat plate affects some core indicators of mortars such as range, shooting accuracy, and maneuverability. In order to withstand huge impact loads, the seat plate was previously made of metal, which accounts for approximately 30%–45% of the total weight of the gun. The drawbacks of the heavy weight of the seat plate, which are not conducive to transportation and transfer, run counter to the current direction of the mortar's lightweight development. The application of composite materials can greatly reduce the weight of the seat plate, but it exacerbates the contradiction between the mobility and combat effectiveness of mortars. In order to achieve the best match between mortar stability and maneuverability, a multiobjective optimization of composite material layers for seat plates is proposed, utilizing the designability of composite material layers. First, a fiber continuity model based on dropout sequence is adopted to solve the problems existing in the design of inherent continuity classes for composite layered fibers. Second, a hybrid surrogate model that considers the composite material seat plate quality, structural strength, shooting stability, shooting accuracy, and various working conditions is considered. Then, in order to improve the optimization efficiency and robustness of the algorithm, a multiobjective optimization algorithm based on the Chebyshev combination pattern is used to solve the mixed surrogate model. Finally, the optimization results are comprehensively evaluated against the optimization objectives. Research has shown that the method proposed in this article can effectively solve the time-consuming problem of multiobjective optimization, improve the accuracy of hybrid surrogate models, and meet the expected requirements of multiobjective optimization of composite material seat plates. While ensuring shooting stability, the weight of the seat plate is reduced by 18.43% compared to the metal seat plate, which has important application value for lightweight design of mortars.

## 1. Introduction

Mortar is a type of artillery with a special trajectory that plays a huge role in complex terrain combat environments, such as mountains, hills, and cities. As an important force transmission component of mortars, the seat plate affects the core indicators of mortar range, shooting accuracy, and maneuverability. Due to the need to withstand huge impact loads, the seat plate was previously made of metal, which accounts for approximately 30%–45% of the total weight of the gun. The drawbacks of heavy weight of the seat plate, which are not conducive to transportation and transfer, run counter to the current direction of the mortars lightweight development. Therefore, while meeting the requirements of intensity and shooting stability, reducing the weight of the seat plate as much as possible is an urgent technical challenge. It can facilitate rapid disassembly and assembly, human and animal carrying, vehicle transportation, and paratroopers' airborne and airdrop and improve the mortar's rapid mobility and combat capability.

Composite materials are widely used in various fields due to their advantages such as lightweight, high strength, design ability, and good impact performance and are considered to be helpful in solving the problem of lightweight design of seat plates [1]. However, the design of composite material structures requires the layer structure

determination of the laminated plate, including the number of layers, the thickness of each layer, and the laying angle. Compared to the metal structure design, more design variables are required. Moreover, the optimization of the laying angle includes discrete variables [2]. Although the application of composite materials can reduce structural mass, but the material characteristics of composite materials make the structural nonlinear problem in mortar systems more prominent than conventional ground guns, and the contradiction between mortar mobility and combat effectiveness has become increasingly acute.

In order to match multiple objectives of mortars, Zhang et al. [3] applied the multiobjective optimization to the optimization of seat plates. Ma [4] established finite element models of the underground seat plates of different shooting arrays and applied software platform integration to implement multiobjective optimization of the parameterized model. Based on the multiobjective optimization theory of the genetic algorithm, Zhou [5] studied the optimization space and effectiveness of the antirecoil device under the simultaneous consideration of the structure of multiple working conditions and overall integration. Jia [6] used the Ansys Workbench finite element engineering technology simulation platform to carry out the structural lightweight design and material lightweight design on the seat plate. Wang et al. [7] used the optimization method of the lightweight composite material layer to carry out the lightweight design of the mortar seat plate. Ge et al. [8] used carbon fiber reinforced resin matrix composite materials as the main body of the seat plate to absorb recoil energy through large deformation dispersion.

In fact, the ultimate goal of composite structure optimization is to specify a layer structure for each design area. When regions are designed independently, conflicting layup angles may occur, resulting in the fibers no longer being continuous. Stress concentrations near the region boundaries due to the cut-off of the force transmission paths can affect structural safety and workmanship. To this end, certain rules are used to transform the independently designed layers of each area into designs that meet fiber continuity constraints. Stodieck et al. [9] introduced the concepts of design variable zones and sublaminates for the fiber continuity design of composite materials. Irisarri et al. [10] used a shared-layer blending model to achieve fiber continuity adjustment in adjacent regions after obtaining the number of layers in each region for each fiber angle. Kristinsdottir et al. [11] introduced a method where each layer originates from a critical or thickest region and can continuously cover any number of adjacent regions. Yang et al. [12] introduced the concept of ply drop sequence (PDS) into the design of multiregion composite laminates. He used genetic algorithm (GA) with special operators and coding methods for PDS-based hybrid optimization, which ensures that the design is fully hybridized during the GA iteration process.

At the same time, the optimization problem of composite materials often has multiple objective functions, and the solution of these objective functions often requires time-consuming simulation calculations. The vast majority of optimization algorithms currently employed are multiobjective optimization algorithms based on various surrogate models [13], such as polynomial response surface (PRS) [14], radial basis function (RBF) [15], and Dou et al.'s [16] support vector regression (SVR). [17]. For different types of optimization problems, different surrogate model methods have their own advantages and disadvantages and exhibit varying performance in model accuracy, optimization efficiency, and robustness. A fuzzy clustering algorithm based on a single alternative model was tested using a synthetic dataset by Shi et al. and the membership of the data and the weights of the surrogate model were obtained [18]. Ariyarit et al. adopted a multifidelity optimization technique that exploits the efficient global optimization capability of a hybrid agent model to solve helicopter blade design problems. This model uses the Kriging method to construct local deviations and uses radial basis functions to construct the global model. The optimization results were compared with those of the ordinary Kriging method and the co-Kriging method, and the best solution was obtained [19]. Sun et al. studied the construction method of a mixed substitution model based on second-order polynomial response surface models (PRSMs), radial basis functions (RBFs), and Kriging lattice substitution models for the multiparameter optimization problem involved in the pulse jet cleaning process of bag filters [20]. Liu et al. proposed a new alternative model PC-GK-SBL, which combines polynomial chaotic expansion (PCE) and Gaussian kernel (GK), under the sparse Bayesian learning (SBL) framework, significantly improving computational efficiency [21]. Denimal et al. combined the Kriging form with generalized polynomial chaos to predict friction-induced instability with interval and probability uncertainties [22]. Li et al. proposed a global optimization algorithm based on the adaptive weighted hybrid surrogate (GOA-AWHS) model. In each iteration, a hybrid model based on the Kriging method and RBF is constructed by adaptively selecting weight coefficients. Then, the prediction target, root mean square error, and distance parameter are optimized to generate Pareto boundaries. Finally, further selecting data points at the Pareto frontier can yield multiple promising optimal solutions [23]. Similar research has also shown that a hybrid surrogate model (HSM) is used to improve the RDO efficiency of partially ribbed shells [24]. Zerpa et al. [25] used polynomial regression surrogate (PRS), radial basic function (RBF), and KRG surrogate models to obtain a mixed surrogate model by linearly stacking them with a certain weight factor and applied it to the optimization of ternary composite flooding oil recovery programs. Goel et al. [26] proposed a heuristic weight factor calculation method, where the weight coefficients are determined by the prediction sum of squares (PRESS) calculated from the test samples. Zhang et al. [27] combined two weight factor calculation methods to balance the global search ability and local exploration ability of optimization methods. Long et al. [28] proposed a multiresponse weighted adaptive sampling (MWAS) method based on a hybrid surrogate model to improve the fitting accuracy and optimization efficiency of the surrogate model and applied it to the multiobjective lightweight design of car seats.

Therefore, the abovementioned methods have significant application value, but in previous studies, relevant methods have not been introduced into the multiobjective optimization research of mortar composite material seat plates. In this context, this article conducted research on the optimization of mortar composite material seat plates based on a multiobjective optimization algorithm by using a hybrid surrogate model. The structure of this article is shown in Figure 1.

First, the preparatory work includes the establishment of a finite element model for composite material seat plates. A fiber continuity model based on the dropout sequence is used to solve the problems in the inherent continuity class design method of composite material layer fibers. A preliminary verification of the model is carried out through modal experiments. Second, the BP neural network surrogate model and the Kriging surrogate model were established, and a hybrid surrogate model method based on the Chebyshev combination pattern was adopted. The application of the hybrid surrogate model method based on the Chebyshev combination pattern, the augmented Tchebycheff-assisted ensemble surrogate multiobjective optimization (ATAESMO)method [29], was considered for solution. Through testing the feasibility of the method, the optimization efficiency and robustness of the algorithm were improved. Then, the abovementioned models and methods were applied to study the optimization of layer thickness under multiobjective matching of composite material seat plates. The weight of the seat plates was minimized while meeting the design requirements of strength, deformation, and shooting stability. The research results indicate that the research ideas and methods in this article have good results in the lightweight of mortars and have certain reference value for improving the maneuverability of mortars.

## 2. Preliminary

*2.1. Description of Laminated Structure of Multiregion Composite Materials.* In addition to the fiber continuity criterion, the layup of composite materials also needs to follow the general principles [30] and the load-bearing characteristics of the seat plate. The layup method of $(+45^{\circ}/-45^{\circ}/0^{\circ}/90^{\circ}/-45^{\circ}/+45^{\circ})$ is preliminarily selected. In these layers, the $0^{\circ}$ layer mainly bears axial loads; the $\pm 45^{\circ}$ layer mainly ensures the shear modulus of the material model to improve the stability and impact resistance of the structure and reduce the stress concentration; and the $90^{\circ}$ layer mainly bears lateral loads to control the Poisson effect [31].

At present, in order to improve the manufacturability of multiregion composite laminated structures and reduce stress concentration in the structure, certain rules are generally set in advance during the layer design process. They would help to guide the appearance of fiber continuity layers, avoid inefficient search, and improve the design effect of the layer. The biggest limitation of the commonly used classic-guided continuity model lies in its strict layer dropping rules, which make the model concise and efficient in design. Adopting loose dropout rules can certainly expand the feasible design space, but determining the next dropout position poses difficulties for the implementation of the rules. Therefore, the sequence of dropouts is the key to defining a continuity model. This article adopts a fiber continuity model based on dropout sequences, combines dropout sequences that define dropout rules with classical-guided continuity models, and achieves the description of multiregion layered structures under loose dropout rules.

The construction method of layer dropping sequence is as follows: we suppose that there are laminated plates with $N$ layers in the structure, where each single layer corresponds to a unique positive integer representing its position in the thickness direction of the laminated plate. For example, from top to bottom, each single layer can be numbered sequentially with the numbers from 1 to $N$. After numbering, we put the number corresponding to the first interrupted single layer when the thickness becomes smaller into the leftmost end of the layer loss sequence. Then, we put the number of subsequent interrupted single layers into the layer loss sequence in turn (just to the right of the previous number), until the last number is placed into the rightmost end of the layer loss sequence [32]. In this way, the specific layer loss rules can be obtained by simply reading the layer loss sequence from left to right. Figure 2 lists two layer loss sequences.

The three main areas of the composite material seat plate, the main plate, the conical basin, and the back plate are represented by $A$, $B$, and $C$, respectively, as shown in Figure 3. Assuming that the number of plies of the three laminates is 3, 4, and 2, respectively, a positive integer sequence (123456) is used to represent the positions of the six single layers in the thickness direction (from top to bottom) in the wizard, respectively. For the four single layers in $B$, their ply angles correspond to four single layers in the wizard, which means that two single layers should be deleted from the wizard with a thickness of six layers. By using the layer dropping rules defined by the layer dropping sequence, the single layer interrupted from the wizard can be determined. Assuming that the layer dropping sequence is (312654), the positions of the two single layers to be deleted in the wizard are 3 and 1, respectively, and the corresponding ply angles are $-45^{\circ}$, $90^{\circ}$ and $45^{\circ}$, respectively. After eliminating these two layers from the wizard, the remaining layer order is (45 0 0 90), which is also the layer structure of plate $B$. Similarly, after deleting the 3# and 6# plies (i.e., $0^{\circ}$ and $90^{\circ}$ plies) in turn, the ply structures of plate $A$ and plate $C$ are (45 −45 90) and (45 −45), respectively.

*2.2. Finite Element Model of Composite Material Seat Plate.* As a weapon system, the most important component of a mortar is the launch system, which is composed of a recoil part (barrel and tail, loading mechanism, seat plate, and surrounding soil), an aiming part (high and low aircraft, directional aircraft, and sight glass), and a frame part. When a mortar is fired, the pressure of gunpowder gas acts on the bottom of the gun chamber to push the recoil part to recoil along the load transmission path. The firing load is transmitted to the tail of the gun through the barrel and then to the ground through the seat plate. Based on the topology

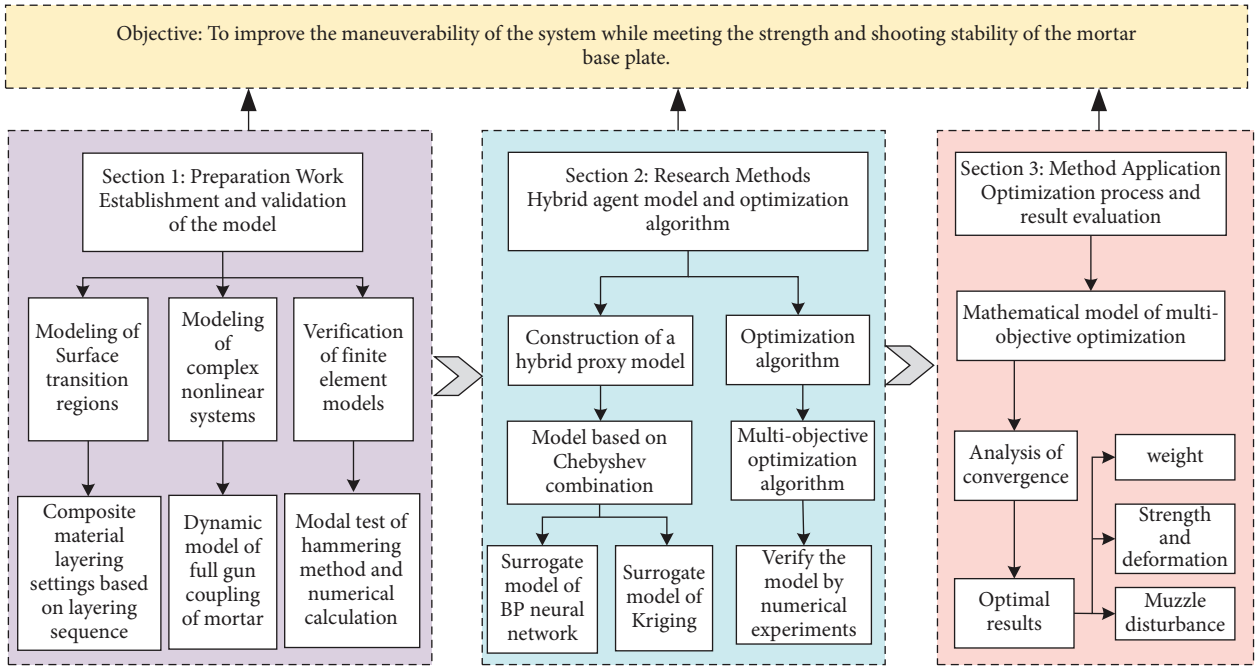


Figure 1: The research ideas of this article.

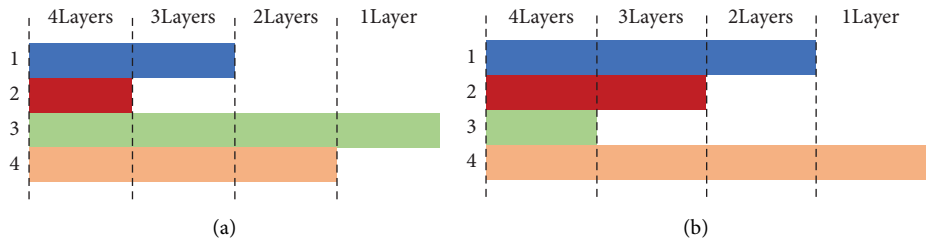


Figure 2: The schematic diagrams of layer dropping sequences: (a) 2 1 4 3 and (b) 3 2 1 4.

optimization results of the seat plate and the structural characteristics of the trapezoidal pyramid seat plate, the load-bearing skeleton of the main plate, conical basin, and back plate in the seat plate is designed, which is still made of the titanium alloy material [33]. A coordinate system is established at the center point of the barrel muzzle: the x-axis is perpendicular to the barrel ground plane, the y-axis is the axis direction of the mortar barrel, and the z-axis is determined according to the right-hand spiral rule; a coordinate system 2 is established at the center position of the seat plate in the mortar: the axis is horizontal and transverse, the axis is vertical and downward, and the axis is horizontal and longitudinal. The established dynamic model of a mortar coupled with composite material seat plate and soil is shown in Figure 4.

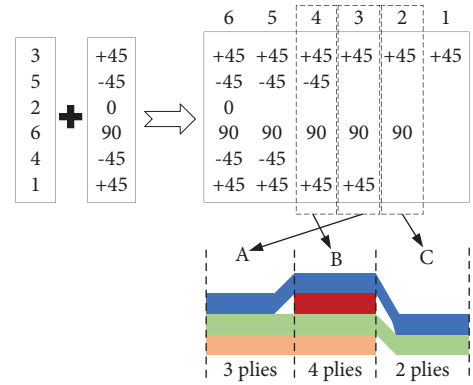


Figure 3: The schematic diagram of the fiber continuity model based on layer dropping sequence.

*2.3. Modal Analysis and Experimental Study of Composite Material Seat Plate.* To preliminarily verify the reliability of the model, a modal testing system was used to conduct modal tests on the composite material seat plate, as shown in Figure 5. In order to ensure that the free boundary conditions of the calculated and experimental modes are consistent, the suspension method is used in the experimental mode analysis to simulate the free boundary. The composite material seat plate belongs to the welded structure of titanium alloy and carbon fiber and has good linear dynamic characteristics, so hammering excitation is adopted. According to simulation calculations, it can be seen that

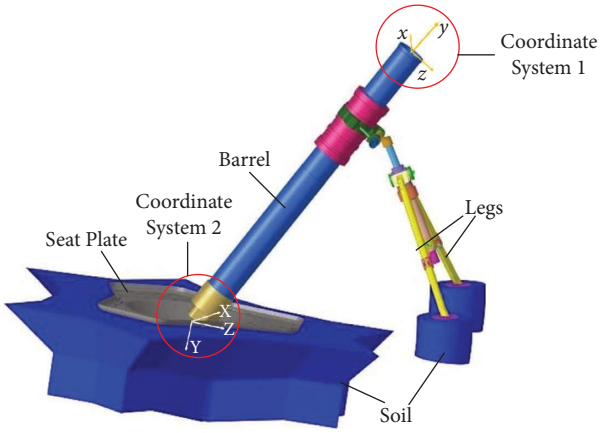


Figure 4: The coupling model of mortar composite material seat plate and soil.

the seat plate is subjected to the maximum force around the joint. Test points are arranged in such areas for easy measurement and identification. A total of 16 excitation points are arranged in the experiment.

After multiple tests, signals from 16 points were collected and frequency domain fitting analysis was performed on the data using the PolyLSCF modal identification method. Under SUM function identification, various modal parameters were obtained, and the vibration mode was estimated by using the least squares frequency domain method. In the simulation calculation, free boundary conditions are set to obtain the frequency comparison between the first 5 modal calculation modes and experimental modes of the composite material seat plate, as shown in Table 1.

According to Table 1, the maximum absolute error between the calculated natural frequency value and the experimental value is 3.42%. The reason for the error is, on the one hand, that the material properties used in the calculation mode assume that the structure is uniform and dense, without pores and cracks, which is different from the actual object. Additionally, the composite material seat plate has an anisotropic material structure, which can bring errors to the calculation. On the other hand, due to the influence of environmental and equipment factors, especially the noise interference during the testing process, relative errors can also be generated. However, the overall relative error is less than 5%, which is within an acceptable range. It can be considered that the two have a good consistency, and the established finite element analysis model has a good accuracy.

## 3. Multiobjective Optimization Method for the Mixed Surrogate Model

*3.1. Hybrid Surrogate Model.* Directly adopting complex and high-precision original simulation models leads to a significant increase in single calculation costs and computational complexity, making it difficult to obtain optimization results within an acceptable range of calculation costs. Therefore, using a surrogate model with high computational efficiency to replace a complex high-precision simulation model is a widely accepted and effective solution. We set $\mathbf{x} = (x_1, x_2, \cdots, x_n)^T$ as an $n$-dimensional input variable, and $y$ is the output variable. For $N$ sets of training sample data $\mathbf{X} = (\mathbf{x}^1, \mathbf{x}^2, \cdots, \mathbf{x}^N)^T$, its corresponding target response value is $Y = (y^1, y^2, \cdots, y^N)^T$. By using different surrogate model functions, the relationship between input variable $x$ and output $y$ response can be approximated as follows [34]:

$$y = f(x) + \varepsilon, \tag{1}$$

where $\varepsilon$ is the random error of approximation $f(x)$ to $y$.

*3.1.1. BP (Backpropagation) Neural Network Surrogate Model.* BP neural networks are generally composed of input layer, hidden layer, and output layer, as shown in Figure 6.

Before using the BP neural network for prediction, it is necessary to first conduct network training, which mainly includes the steps shown in Figure 7.

*Step 1.* The number of input layer nodes $n$, hidden layer nodes $h$, and output layer nodes $m$ are determined. The weights between the input layer and the hidden layer $w_{ji}$, the weights between the hidden layer and the output layer $\theta_j$, the hidden layer threshold, and the output layer threshold $\theta_k$ are initialized. The appropriate learning rate $\eta$ and activation function are selected.

*Step 2.* Forward propagation calculation: in this step, the input information is processed layer by layer from the input layer through the hidden layer and then transmitted to the output layer. The state of each layer's neurons only affects the state of the next layer's neurons.

*Step 3.* Error calculation: the error between the predicted output $y_k$ and the expected output $t_k$ of the neural network output layer is calculated.

*Step 4.* The weights and thresholds of the output layer and hidden layer are updated.

*Step 5.* We determine whether the prediction accuracy of the neural network surrogate model meets the requirements. If it does not meet the requirements, then Steps 2 to 4 are repeated.

From the abovementioned training steps, it can be seen that the BP neural network adjusts the network weight and threshold to reduce the error of the network's prediction output along the gradient direction until it reaches the expected prediction accuracy or the number of iterations exceeds the set value.

*3.1.2. Kriging Surrogate Model.* The Kriging surrogate model is an interpolation model whose interpolation result is defined as a linear weighting of the response values of the known sample function.

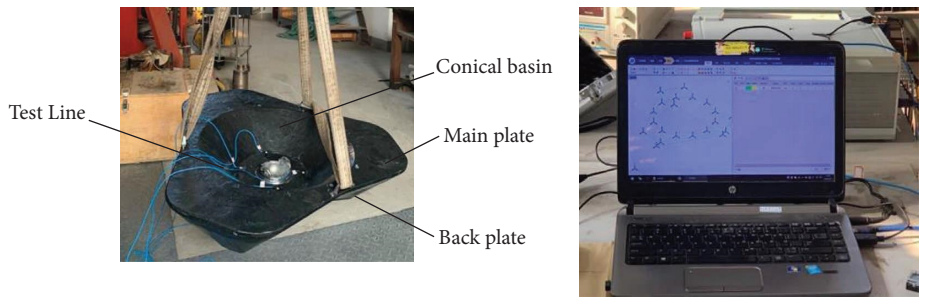


Figure 5: The modal test: (a) the testing ground and (b) the test interface.

Table 1: The comparison of frequencies between calculated and experimental modes.

| Order | Experimental modal values (Hz) | Calculated modal values (Hz) | Relative error (%) |
|---|---|---|---|
| 1st | 679.97 | 660.07 | −2.93 |
| 2nd | 692.62 | 689.47 | −0.45 |
| 3rd | 714.57 | 702.14 | −1.74 |
| 4th | 749.30 | 723.69 | −3.42 |
| 5th | 851.29 | 827.08 | −2.84 |

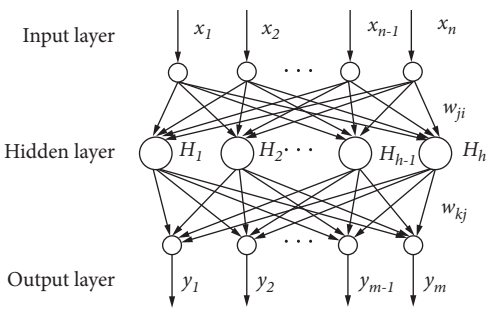


Figure 6: The schematic diagram of BP neural network topology structure.

$$\hat{y}(x) = \sum_{i=1}^{n} \omega^{(i)} y^{(i)}, \qquad \omega = \left[\omega^{(1)} \omega^{(2)} \cdots \omega^{(n)}\right]^T. \tag{2}$$

Therefore, as long as the expression of the weighted coefficient $\omega$ can be given, the performance estimation value of any design scheme in the design space can be obtained. In order to calculate the weighting coefficients, the Kriging model introduces statistical assumptions by treating the unknown function as a specific implementation of a Gaussian static stochastic process. This static random process is defined as follows:

$$Y(x) = \beta_0 + Z(x), \tag{3}$$

where $\beta_0$ is an unknown constant, also known as the global trend model, representing the mathematical expected value of $Y(x)$ and $Z(x)$ represents a static random process with a mean of zero and a variance of $\sigma^2$. At different locations in the design space, these random variables have a certain degree of correlation (or covariance). The covariance can be expressed as follows:

$$\mathrm{Cov}\left[Z(x), Z(x')\right] = \sigma^2 R(x, x'), \tag{4}$$

where $R(x, x')$ is the "correlation function" (only related to spatial distance), and it is equal to 1 when the distance is zero; when the distance is infinite, it is equal to 0; the correlation decreases with increasing distance. Based on the abovementioned assumptions, the Kriging model searches for the optimal weighting coefficient $\omega$ by minimizing the mean square deviation $\hat{y}(x)$ as

$$\mathrm{MSE}[\hat{y}(x)] = E\left[\left(\omega^T Y_S - Y(x)\right)^2\right]. \tag{5}$$

This satisfies the following interpolation conditions (or unbiased conditions):

$$E\left[\sum_{i=1}^{n} \omega^{(i)} Y\left(x^{(i)}\right)\right] = E[Y(x)]. \tag{6}$$

By using the Lagrange multiplier method, it can be proven through derivation that the optimal weighting coefficient $\omega$ is given by the following linear equation system:

$$\begin{cases} \sum_{j=1}^{n} \omega^{(i)} R\left(x^{(i)}, x^{(j)}\right) + \dfrac{\mu}{2\sigma^2} = R\left(x^{(i)}, x\right), \\ \sum_{j=1}^{n} \omega^{(i)} = 1, \end{cases} \tag{7}$$

where $i = 1, 2, \cdots, n$ and $\mu$ is the Lagrange multiplier.

*3.1.3. Hybrid Surrogate Model.* Under the premise of selecting a suitable single surrogate model as its subsurrogate model, determining the hybrid strategy, that is, determining the weight coefficients through effective calculation methods, is the key to the modeling process of the hybrid

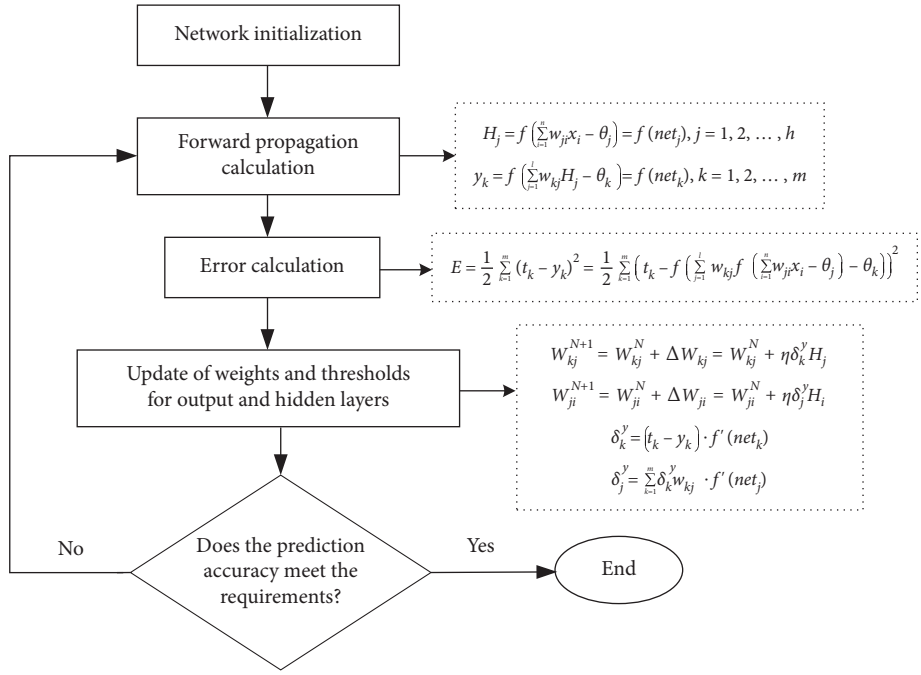


Figure 7: The BP neural network training process.

surrogate model. By combining multiobjective EI criteria for multiobjective optimization [35], the predicted values of multiple surrogate models are used as objective vectors. Although the distribution of predicted values of multiple surrogate models may be uneven, the degree to which it approximates the optimal predicted values of multiple surrogate models is very high [36]. The formula is expressed as follows:

$$\hat{y}_i(x) = \max_{1\le j\le m}\left\{\lambda_j \cdot \hat{f}_i(x)\right\} + \lambda_{\min}\sum_{j=1}^{m}\lambda_j \cdot \hat{f}_i(x), \quad (8)$$

where $\hat{y}_i(x)$ represents the predicted value of the $i$-th objective function; $m$ represents the number of surrogate models; $j$ represents the predicted value of the $j$-th surrogate model at point $x$; and min is the minimum value of the weight coefficient. The BP neural network surrogate model and the Kriging surrogate model selected in this article are combined to predict the objective function value. The weight of each subsurrogate model in the mixed surrogate model will be calculated according to the following equation:

$$\lambda_i = \frac{E_i^{-1}}{\sum_{i=1}^{m} E_i^{-1}}, \quad (9)$$

where $E_i$ is the approximate capability evaluation value of the subagent model and we selected the root mean square error (RMSE) as $E$.

*3.2. Optimization Algorithm.* To address the time-consuming multiobjective optimization design problem and improve the optimization efficiency of the multiobjective EGO algorithm, this article adopts the ATAESMO algorithm, whose main process is shown in Figure 8.

First, we determine the objective function based on the initial sample set. Then, we establish BP neural network surrogate models, Kriging surrogate models, and their hybrid surrogate model to evaluate the accuracy of the hybrid surrogate model of the two surrogate models. Then, based on the expected volume improvement formula, the current optimal solution is obtained, and the sampling points are updated to determine whether the iteration stop criteria are met. If not, then the updated sampling points will be added to the established surrogate model [37, 38]. At present, the multiobjective improvement function that has been extensively studied is the hypervolume improvement function, and the single objective expected improvement (EI) criterion is extended to the multiobjective EI criterion combined with surrogate model methods to optimize multiobjective optimization problems. The multiobjective EI criterion is used to measure the improvement value of the unknown point $X$ on the current nondominated frontier solution, expressed by the following formula [39]:

$$I_h(X) = H(S \cup X) - H(S), \quad (10)$$

where $S$ represents the current nondominated frontier and $H$ represents the hypervolume index of the nondominated frontier. The physical meaning of the hypervolume index is the volume of a closed area composed of a nondominant front and a reference point, which is defined as follows:

$$H(S) = \text{volume}\{y \in R \mid S \prec y \prec r\}, \quad (11)$$

where $r$ is the reference point specified by the user and must be dominated by all nondominated frontier solutions. The formula for calculating the expected volume improvement is as follows:

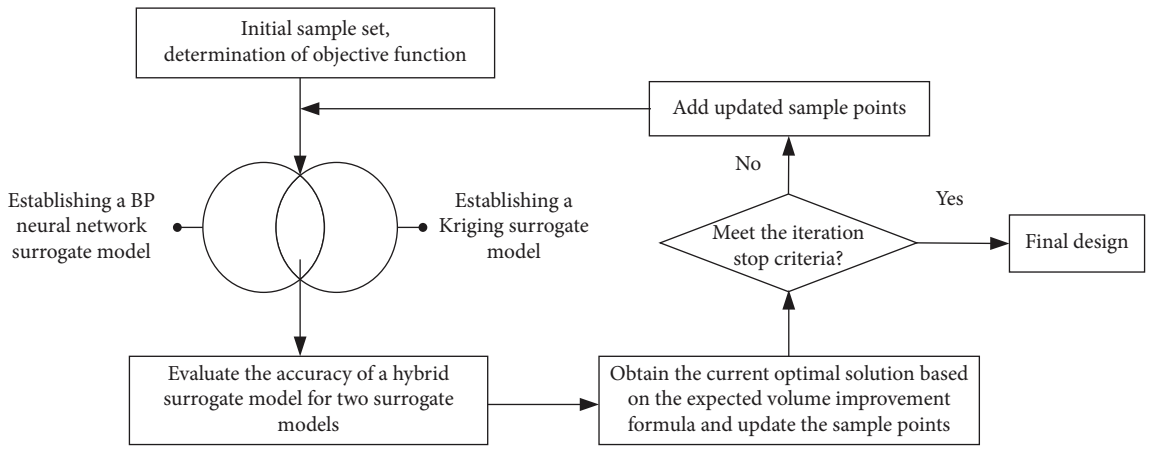


Figure 8: The flow of the ATAESMO algorithm.

$$S = \int_{l_1}^{u_1} \cdots \int_{l_m}^{u_m} I([y_1, \cdots, y_m], P) \cdot \phi([y_1, \cdots, y_m]) dy_1 \cdots dy_m. \tag{12}$$

We decompose formula (12) into three terms, namely, $Q_1$, $Q_2$, and $Q_3$:

$$\begin{aligned} Q_1 &= \int_{l_1}^{u_1} \cdots \int_{l_m}^{u_m} \prod_{j=1}^{m} (v_j - y_j) \cdot \phi([y_1, \cdots, y_m]) dy_1 \cdots dy_m \\ &= \prod_{j=1}^{m} \left( \Psi(v_j, u_1, \mu_j, \sigma_j) - \Psi(v_j, l_j, \mu_j, \sigma_j) \right). \end{aligned} \tag{13}$$

The integration formula for the edge normal distribution function is as follows:

$$\Psi(a, b, \mu, \sigma) = \sigma\phi\left(\frac{b-\mu}{\sigma}\right) + (a-\mu)\Phi\left(\frac{b-\mu}{\sigma}\right). \tag{14}$$

Therefore,

$$\begin{aligned} Q_2 &= \int_{l_1}^{u_1} \cdots \int_{l_m}^{u_m} \prod_{j=1}^{m} (v_j - y_j) \cdot \phi([y_1, \cdots, y_m]) dy_1 \cdots dy_m \\ &= \prod_{j=1}^{m} (v_j - u_j) \left( \Phi\left(\frac{u_j - \mu_j}{\sigma_j}\right) - \Phi\left(\frac{l_j - \mu_j}{\sigma_j}\right) \right), \\ Q_3 &= \int_{l_1}^{u_1} \cdots \int_{l_m}^{u_m} \prod_{j=1}^{m} Vol(S) \cdot \phi([y_1, \cdots, y_m]) dy_1 \cdots \mathrm{d}y_m \\ &= \mathrm{Vol}(S) \prod_{j=1}^{m} \left( \Phi\left(\frac{u_j - \mu_j}{\sigma_j}\right) - \Phi\left(\frac{l_j - \mu_j}{\sigma_j}\right) \right). \end{aligned} \tag{15}$$

*3.3. Numerical Experiments.* Before applying the above-mentioned algorithms and hybrid surrogate models to the research object of this article, we compare the ATAESMO algorithm with the Thompson sampling efficient multi-objective optimization (TSEMO) algorithm and the single surrogate multiobjective optimization (SSMO) algorithm.

The TSEMO algorithm establishes a surrogate model based on the Gaussian regression process spectral sampling method and predicts optimization problems. Then, the NSGA-II algorithm is used to optimize the surrogate model and obtain a set of candidate sample points. This algorithm can maximize the optimization of hypervolume improvement and select the next set of optimal solutions. This process continues until the algorithm reaches the predetermined maximum number of samples/iterations. The SSMO algorithm usually only applies a single surrogate model, and other optimization processes are consistent with the ATAESMO algorithm.

Taking the test of a function with a target number of 2 as an example, three benchmark test functions with relatively good performances, ZDT1, ZDT2, and ZDT3, were selected to test the optimization efficiency of the ATAESMO algorithm. The dimensions of the three objective functions were 10, 6, and 10, respectively, all of which had strong nonlinearity, and the true nondominant solution of the selected test function was known [40].

In order to compare the optimization efficiency of optimization algorithms, reference [29] in this article selects the hypervolume index and the inverted generational distance (IGD) index to measure the final approximate nondominated frontier solution. Assuming that the true nondominated frontier of the problem is $P$, and the approximate nondominated frontier obtained by the multiobjective optimization algorithm is $P$, then the IGD calculation formula is

$$\mathrm{IGD} = \frac{\sum_{p \in P^*} d(p, P)}{\left|P^*\right|}, \tag{16}$$

where $d$ is the minimum value of all Euler distances from point $P$ to the nondominated approximation frontier point $P$. Only when the approximate nondominated frontier is very close to the real nondominated frontier and does not miss any part of the real nondominated frontier solution, the IGD index will be relatively small. The larger the hypervolume index value that approximates the nondominant front, the smaller the IGD index value, indicating a higher quality. Table 2 presents the statistical values of the hypervolume index and IGD index obtained by optimizing and iterating the three test functions through three optimization algorithms.

From Table 2, it can be seen that for the IGD index, the ATAESMO optimization method has the smallest mean and square difference values among the three algorithms, indicating that the ATAESMO algorithm finds the best approximate nondominated frontier solution. For the hypervolume index, the mean and square difference are the smallest, and it can also obtain the approximate nondominated frontier solution with the best accuracy since it has been obtained before. Therefore, as shown in Figure 9, the ATAESMO algorithm is already in approximate complete convergence and has good optimization performance in handling multiobjective optimization problems.

## 4. Optimization Process and Result Analysis

### 4.1. Optimization Process

*4.1.1. Mathematical Model.* During the firing process, the movement of the mortar is roughly divided into the acceleration recoil phase, deceleration recoil phase, and reentry phase. To ensure the shooting accuracy of mortars, it is required that the muzzle vibration state, namely, the lateral displacement, longitudinal displacement, lateral angular displacement, and longitudinal angular displacement of the reference point at the muzzle center, remains within a small range. This is a typical multiobjective optimization problem, whose mathematical model established for the optimization problem of composite material seat plates under multiple working conditions and multiobjective conditions can be described as

$$\begin{aligned} &\min y = f(x) = \left[f_1(x), f_2(x)\right], \\ &\quad x = \left[t_1, t_2, t_3\right]^T, t_i^l \le t_i \le t_i^u, i = 1, 2, 3 \\ &S'_{\max} \le S_{\max}, R > 1, \end{aligned} \tag{17}$$

where, $t_1$, $t_2$, and $t_3$ correspond to the composite material layer thickness of the main plate, conical basin, and back plate, respectively, and $t_i^l$ and $t_i^u$ represent the upper and lower limits of the constrained design variables, taking 5 mm and 20 mm, respectively. Due to the main focus being on the contradiction between seat plate mobility and shooting stability, $f_1(x)$ and $f_2(x)$, respectively, represent the effects of corresponding mass and muzzle vibration of the seat plate. $S'_{\max}$ represents the maximum stress value of the composite material seat plate based on multiobjective optimization under multiple working conditions. $S_{\max}$ represents the maximum stress value of the titanium alloy seat plate, with a calculated value of 446 MPa, which represents the strength ratio of composite laminates expressed as

$$R = \frac{\sigma_{\max,i}}{\sigma_i}, \tag{18}$$

where $\sigma_{\max,i}\,(i = 1, 2, 3)$ represents the intensity vector and $\sigma_i$ represents the applied stress vector.

The aggregation of shooting stability targets is represented as follows:

$$f(x_2) = \sqrt{\frac{U_x^2 + U_z^2}{U_{x0}^2 + U_{z0}^2}} + \sqrt{\frac{\theta_x^2 + \theta_z^2}{\theta_{x0}^2 + \theta_{z0}^2}}, \tag{19}$$

where $U_x$ represents the lateral displacement of the muzzle, $\theta_x$ represents the lateral angular displacement, $U_z$ represents the longitudinal displacement, $\theta_z$ represents the longitudinal angular displacement, and 0 represents the initial value.

Taking a typical medium hard soil working condition as an example, the characteristic parameters of the calculation are listed in Table 3.

Table 2: The comparison of hypervolume index and IGD index for test functions.

| Test function | Algorithm | IGD | | Hypervolume | |
|---|---|---|---|---|---|
| | | Mean value | Square difference | Mean value | Square difference |
| ZDT1 | TSEMO | 0.0112 | 0.0125 | 0.0001 | 0 |
| | SSMO | 2.0709 | 0.3521 | 0.0113 | 0.0003 |
| | ATAESMO | 0.0063 | 0.0032 | 0.0001 | 0.0001 |
| ZDT2 | TSEMO | 0.0002 | 0.0001 | 0.0007 | 0.0016 |
| | SSMO | 1.7108 | 0.3896 | 0.0142 | 0.0027 |
| | ATAESMO | 0.003 | 0.0013 | 0.0006 | 0.0001 |
| ZDT3 | TSEMO | 0.0191 | 0.0102 | 0.0005 | 0.0005 |
| | SSMO | 1.7288 | 0.3601 | 0.0126 | 0.001 |
| | ATAESMO | 0.0073 | 0.0033 | 0.0002 | 0.0001 |

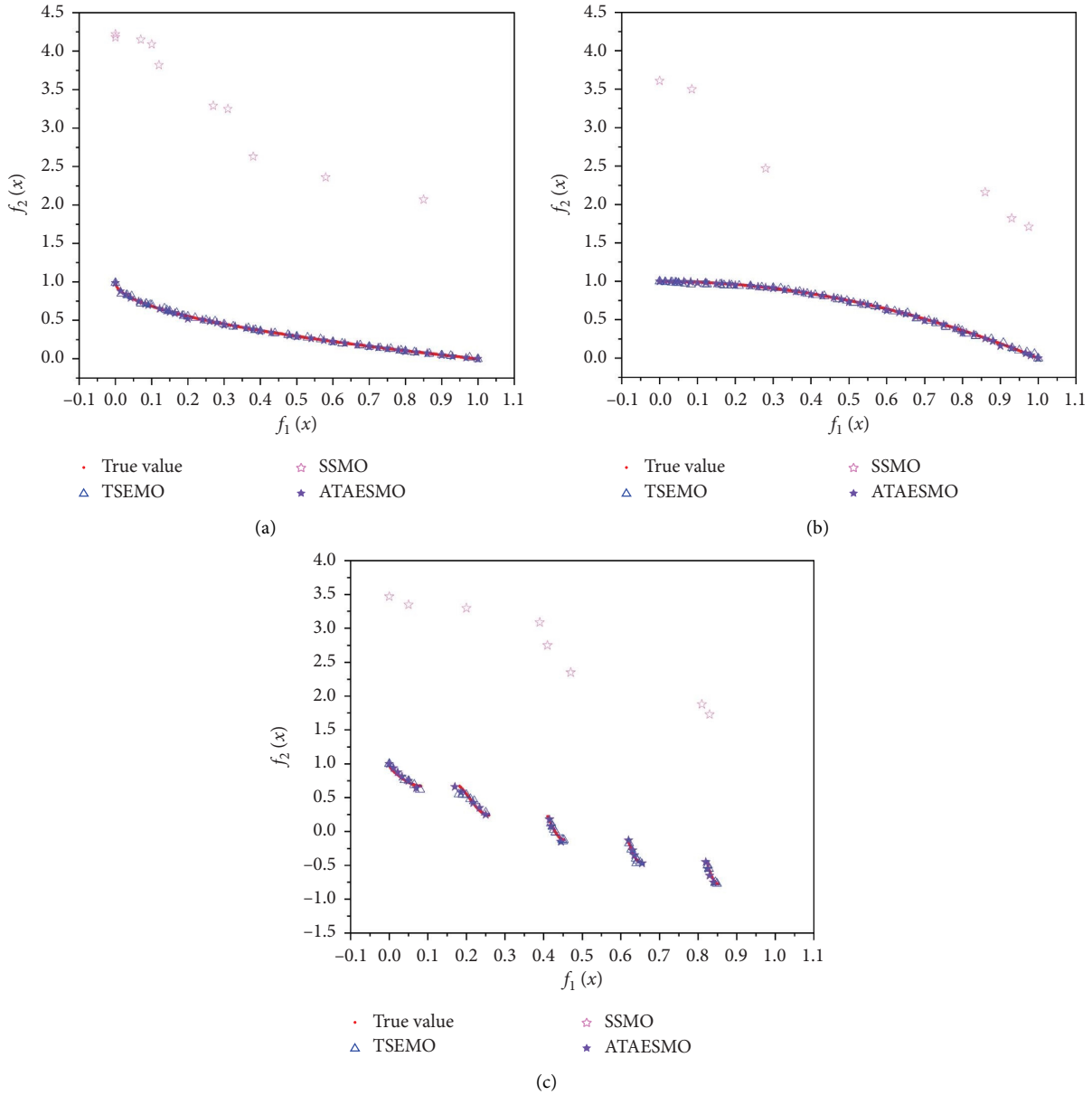


Figure 9: The approximate and true nondominated frontier solutions of the three algorithms: (a) test function is ZDT1, (b) test function is ZDT2, and (c) test function is ZDT3.

Table 3: The parameters of soil working conditions.

| Elastic modulus (MPa) | Poisson's ratio | Density (kg/m$^3$) | Friction angle (°) | Yield stress ratio |
|---|---|---|---|---|
| 100 | 0.29 | 2000 | 8.0 | 0.9 |

*4.1.2. Optimization Processes.* The optimization process is shown in Figure 10. First, we construct a training sample database. Using the optimal Latin hypercube method for experimental design, in addition to the selected three design variables, three operating conditions are needed to be added as variables to the experimental factors. Therefore, during the experimental design, there were a total of 4 factors, including 3 quantitative factors and 1 qualitative factor. 80 sets of training samples were output and substituted into the finite element model of the composite material seat plate full gun for calculation, resulting in the values of each objective.

Second, a hybrid surrogate model is constructed by integrating the BP neural network surrogate model and the Kriging surrogate model. The accuracy of each surrogate model is evaluated, and the final objective function surrogate model is obtained through the Chebyshev combination method for model validation and credibility evaluation.

Then, the ATAESMO multiobjective optimization algorithm is used to solve the optimization problem. We calculate the dynamic response of the optimization solution and determine whether the optimization converges. If it does not converge, then we add the current optimal solution as a new sample point to the sample database, add the updated sample points, and solve the optimization problem again until convergence.

Finally, considering the material characteristics of composite laminates, we determine whether they have failed. If the composite laminates fail, then the optimization calculation will be performed again. If the composite laminates do not fail, then the optimization will be completed.

*4.2. Quality of Seat Plate.* After iterative calculation, the Pareto optimal solution set obtained is shown in Figure 11. From the Pareto solution set, it can be seen that the smaller the mass of the seat plate, the greater the muzzle disturbance. We then analyze the optimization objectives and select the design variables corresponding to the optimal solution.

The comparison of relevant numerical values before and after the optimization of composite materials in the main plate, conical basin, and back plate regions is shown in Table 4.

After optimization, the composite layer thickness of the main plate and conical basin decreased, while the composite layer thickness of the back plate increased. This is because the main plate does not directly bear the impact load, and although the conical basin is connected to the socket, the main force is still borne by the titanium alloy skeleton of the socket and composite material. Therefore, the stress on the composite material in the main plate and conical basin is relatively small. The back of the seat plate interacts with the soil, and the composite material in the back plate has a relatively large area, resulting in a relatively large overall stress. Overall, the optimization results of composite material layer thickness are basically consistent with the stress situation of the mortar seat plate. After design optimization, the mass of the composite material seat plate is 55.76 kg, which is 18.43% less than the 68.36 kg titanium alloy seat plate. The lightweight design effect is obvious.

*4.3. Stress and Deformation of Seat Plate.* We set the firing direction angle of the mortar to 0° and the firing height angle to 85°, calculate the dynamic response of the optimized composite material seat plate, and compare the maximum stress and maximum deformation of the titanium alloy seat plate under the same working conditions with the obtained stress and deformation nephogram, as shown in Figures 12 and 13.

As can be seen from the figure, the force transmission path of the composite material seat plate is clearly displayed, and the use of a layer dropping sequence layer laying method can effectively handle the transition area of the curved surface. The stress in the central area of the composite material seat plate is relatively dispersed, with few stress concentration points, and mainly exists at the connection between the titanium alloy skeleton of the main plate and the composite laminated plate. The maximum deformation of the composite material seat plate mainly occurs in the area of the composite material in the mortar and conical basin, indicating that strong impact loads have a significant impact on the deformation of the center and surrounding areas of the composite material seat plate and have high requirements for the connection between the titanium alloy skeleton and the composite material layer in the composite material seat plate.

Comparing the stress and deformation of the two seat plates, it can be seen that the maximum stress of the composite material seat plate increases by about 5.6% compared to the maximum stress of the titanium alloy seat plate, while the maximum deformation decreases by about 5.9%. This indicates that as the material decreases, the structural strength will indeed be affected, but within the design range and compared to the benefits of weight reduction, it is acceptable. Moreover, the areas with significant stress and deformation in the composite material seat plate are mainly concentrated near the anchorage, while the forces in other areas are more uniform than those in the titanium alloy seat plate, providing a good research foundation for further optimization of the structure.

*4.4. Gun Mouth Vibration.* To test the firing stability of mortars using composite material seat plates, the muzzle vibration of composite material seat plates and titanium alloy seat plates was calculated under the same working conditions. $U_x$, $U_z$, $\theta_x$, and $\theta_z$ are shown in Figure 14.

The moment when the projectile exits the muzzle corresponds to the abscissa of 8.3 ms, marked with a vertical dashed line in the figure. The variation is measured by the difference between the corresponding distance between

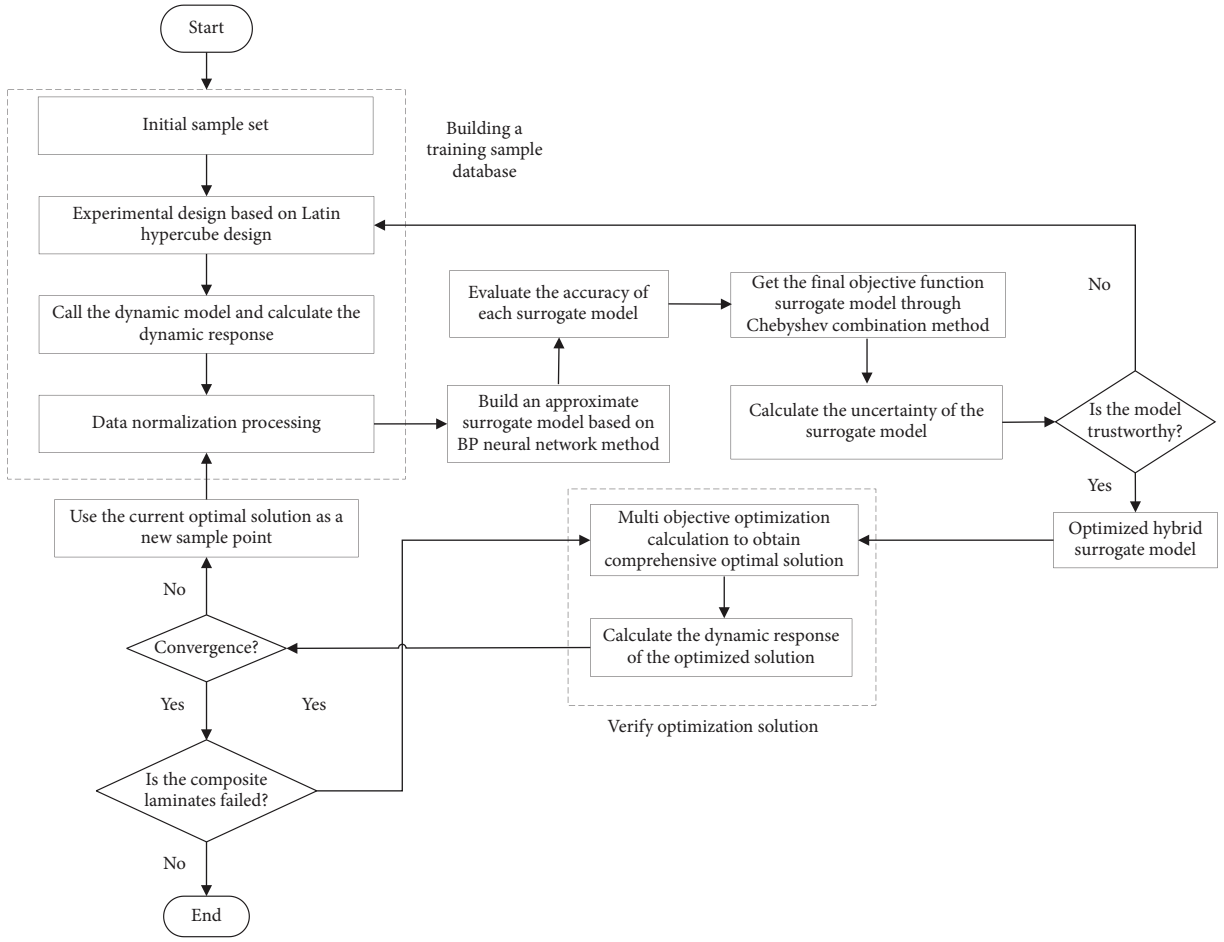


Figure 10: The optimization process.

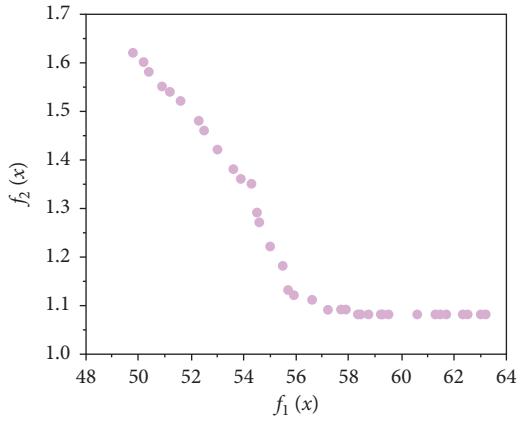


Figure 11: Set of Pareto solution.

the composite material seat plate and the titanium alloy seat plate from the center position (the muzzle does not vibrate). It can be seen that the variation trend of the muzzle vibration of the two types of seat plates has good consistency, and their variation patterns are relatively similar. The difference in the vibration amount when exiting the muzzle is controlled within a small range. This indicates that although the composite material seat plate reduces weight, it does not significantly increase the vibration of the mortar muzzle. Optimization research on the composite material seat plate is beneficial for reducing the muzzle vibration under comprehensive working conditions, creating favorable conditions for improving the accuracy level of mortar firing.

Table 4: The comparison of numerical values before and after optimization.

| Region | Main plate | Conical basin | Back plate |
|---|---|---|---|
| Before optimization (mm) | 7.0 | 7.0 | 7.0 |
| After optimization (mm) | 6.5 | 6.4 | 9.3 |

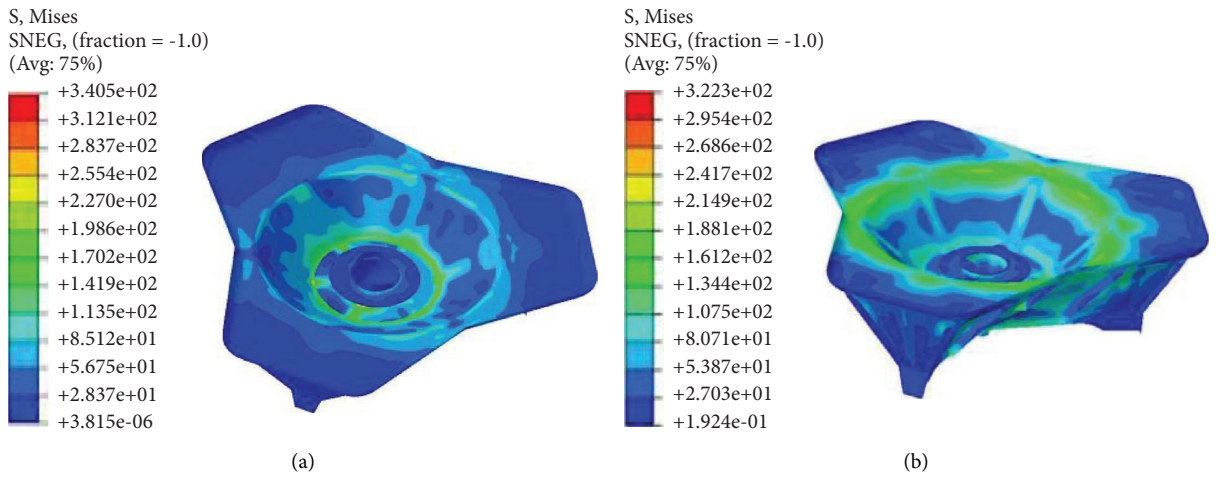


Figure 12: The comparison of stress nephogram: (a) the optimized composite material seat plate and (b) the titanium alloy seat plate.

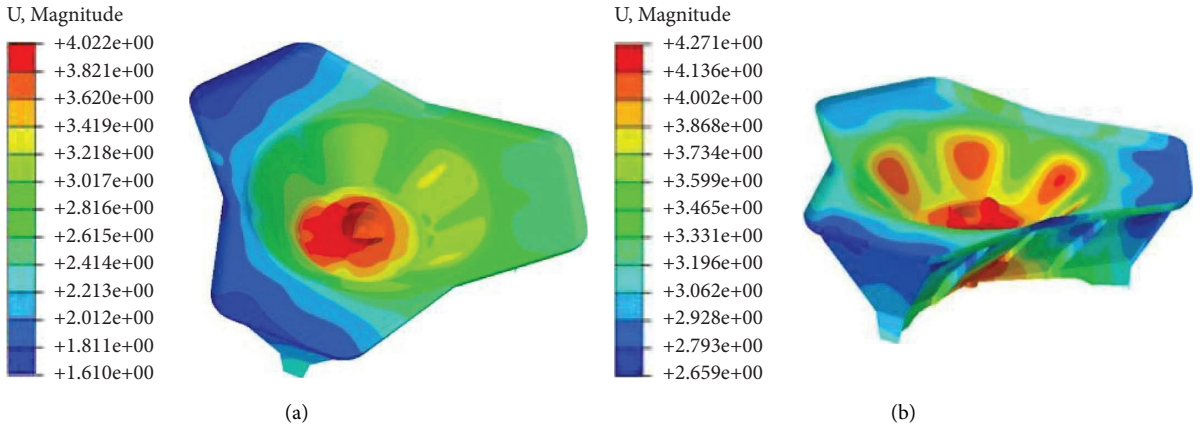


Figure 13: The comparison of deformation nephogram: (a) the optimized composite material seat plate and (b) the titanium alloy seat plate.

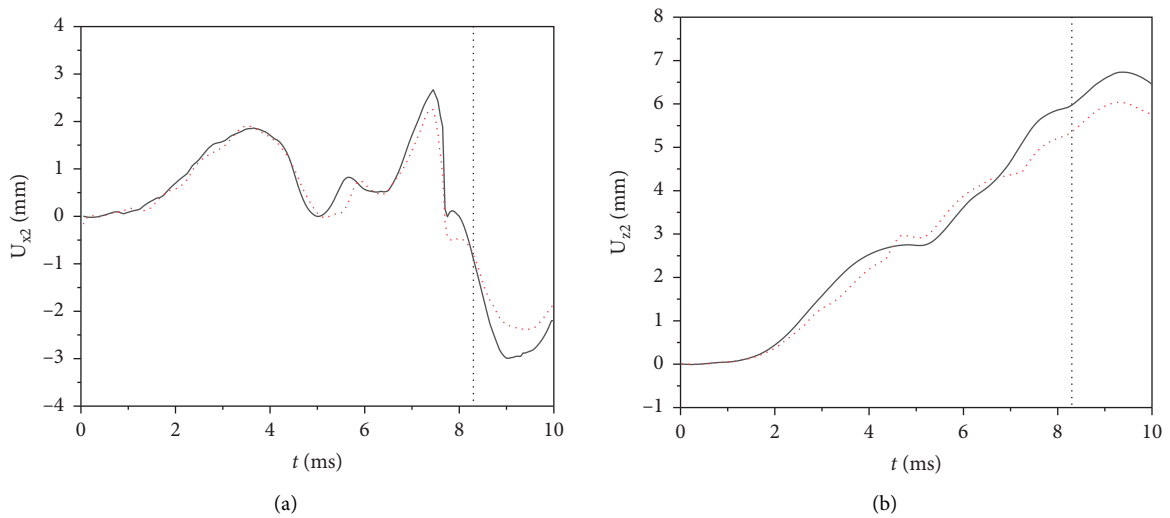


Figure 14: Continued.

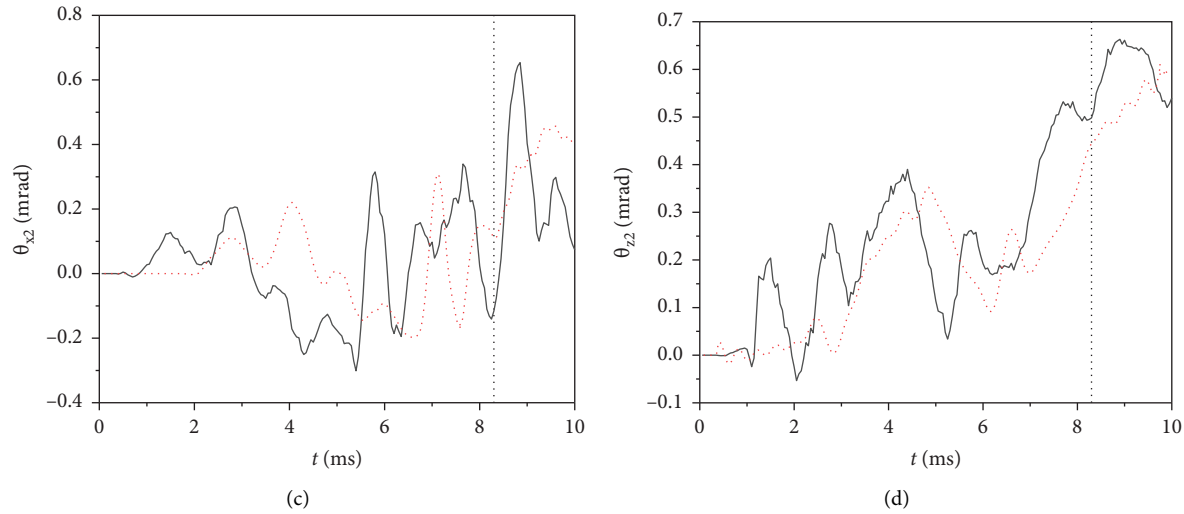


Figure 14: The comparison of muzzle vibration between composite and titanium alloy seat plates: (a) lateral displacement, (b) longitudinal displacement, (c) lateral angular displacement, and (d) longitudinal angular displacement.

## 5. Conclusion

Mortars, due to their unique operational advantages, will still play a significant role in future wars. In order to achieve the lightweight design goal of mortars, a composite material was used to optimize the structure of the seat plate, which accounts for a large proportion of mortars. The main conclusions of this study are as follows: [41].

(1) The use of a fiber continuity model based on dropout sequence can help solve the problems in the inherent continuity class design method of composite laminates, improve the manufacturability of multiregion composite laminates, reduce stress concentration in the structure, and improve the design effect of laminates.

(2) Establishing an accurate finite element model of composite material seat plates is a prerequisite for research. Modal experiments are conducted by simulating free boundaries through suspension, and the PolyLSCF modal identification method is used to perform frequency domain fitting analysis on the data. Under SUM function identification, various modal parameters are obtained. Comparing the experimental mode with the calculated mode can help verify the accuracy of the finite element model.

(3) Adopting a hybrid surrogate model method based on the Chebyshev combination pattern can not only save computational costs but also take into account the predictive characteristics of multiple surrogate models, improving the computational accuracy of the model. By comparing and optimizing the quality, stress, deformation, and shooting stability of the front and rear seat plates, the research results show that this method is feasible and can help achieve the best match between the maneuverability and structural performance of the seat plates. It has a significant reference value for multiobjective optimization and lightweight design of mortar seat plates.

## Data Availability

The data used to support the findings of this study are included within the article.

## Conflicts of Interest

The authors declare that they have no conflicts of interest.

## Acknowledgments

This work was partially supported by the National Natural Science Foundation of China (Grant no. 52305155) and the High Level Talent Research Foundation of the Jinling Institute of Technology (Grant no. jit-b-202227).

## References

[1] E. J. Riley, E. H. Lenzing, and R. M. Narayanan, "Characterization of carbon fiber composite materials for RF applications," *Radar Sensor Technology XVIII International Society for Optics and Photonics*, vol. 9077, 2014.

[2] J. J. Espadas-Escalante, B. A. Bednarcyk, E. J. Pineda, and P. Isaksson, "Modeling the influence of layer shifting on the properties and nonlinear response of woven composites subject to continuum damage," *Composite Structures*, vol. 220, no. 6, pp. 539–549, 2019.

[3] X. M. Zhang, S. H. Liu, K. X. Peng, and S. H. Liu, "Topological optimization design of a mortar pedestal plate," *Journal of Ordnance Equipment Engineering*, vol. 37, no. 4, pp. 33–35, 2016.

[4] H. F. Ma, "Structural analysis and optimization design of mortar pedestal plate," Master's Thesis, Nanjing University of Technology, Nanjing, China, 2009.

[5] L. Zhou, *Research on Multiobjective Optimization Design of Recoil Device for Large Caliber Artillery*, Nanjing University of Technology, Nanjing, China, 2015.

[6] X. L. Jia, *Lightweight Design of Mortar Pedestal Plate Structure*, North University of China, Taiyuan, China, 2019.
[7] X. Y. Wang, J. L. Ge, G. L. Yang, Z. Wang, and F. F. Wang, "Lightweight design of mortar base plate," *Journal of Gun Launch and Control*, vol. 39, no. 4, pp. 56–61, 2018.
[8] J. L. Ge, X. Y. Xie, G. Z. Liu, and G. L. Yang, "Dynamic response analysis and structural optimization of composite seat plates," *Journal of Ballistics*, vol. 32, no. 4, pp. 83–90, 2020.
[9] O. Stodieck, J. E. Cooper, P. Weaver, and P. Kealy, "Optimization of tow-steered composite wing laminates for aeroelastic tailoring," *American Institute of Aeronautics and Astronautics Journal*, vol. 53, no. 8, pp. 2203–2215, 2015.
[10] F. X. Irisarri, A. Lasseigne, F. H. Leroy, and R. Le Riche, "Optimal design of laminated composite structures with ply drops using stacking sequence tables," *Composite Structures*, vol. 107, no. 7, pp. 559–569, 2014.
[11] B. P. Kristinsdottir, Z. B. Zabinsky, M. E. Tuttle, and S. Neogi, "Optimal design of large composite panels with varying loads," *Composite Structures*, vol. 51, no. 1, pp. 93–102, 2001.
[12] J. B. Yang, B. F. Song, X. P. Zhong, and P. Jin, "Optimal design of blended composite laminate structures using ply drop sequence," *Composite Structures*, vol. 135, no. 1, pp. 30–37, 2016.
[13] S. Razavi, B. A. Tolson, and D. H. Burn, "Review of surrogate modeling in water resources," *Water Resources Research*, vol. 48, no. 7, pp. 1–94, 2012.
[14] Y. H. Li, J. J. Shi, H. Cen, J. Shen, and Y. Chao, "A kriging-based adaptive global optimization method with generalized expected improvement and its application in numerical simulation and crop evapotranspiration," *Agricultural Water Management*, vol. 245, pp. 106623–106631, 2021.
[15] M. Rashki, H. Azarkish, M. Rostamian, and A. Bahrpeyma, "Classification correction of polynomial response surface methods for accurate reliability estimation," *Structural Safety*, vol. 81, pp. 101869–101871, 2019.
[16] S. Q. Dou, J. J. Li, and F. Kang, "Health diagnosis of concrete dams using hybrid FWA with RBF-based surrogate model," *Water Science and Engineering*, vol. 12, no. 3, pp. 188–195, 2019.
[17] Y. Hamed, A. Ibrahim Alzahrani, A. Shafie, Z. Mustaffa, M. Che Ismail, and K. Kok Eng, "Two steps hybrid calibration algorithm of support vector regression and K-nearest neighbors," *Alexandria Engineering Journal*, vol. 59, no. 3, pp. 1181–1190, 2020.
[18] M. L. Shi, Z. H. Wang, and L. Z. Xu, "A fuzzy clustering algorithm based on hybrid surrogate model," *Journal of Intelligent and Fuzzy Systems*, vol. 42, no. 3, pp. 1963–1976, 2022.
[19] A. Ariyarit, M. Sugiura, Y. Tanabe, and M. Kanazaki, "Hybrid surrogate-model-basedmulti-fidelity efficient global optimization applied to helicopter blade design," *Engineering Optimization*, vol. 50, no. 6, pp. 1016–1040, 2018.
[20] S. Sun, L. Liu, Z. Yang et al., "Optimization method based on hybrid surrogate model for pulse-jet cleaning performance of bag filter," *Energies*, vol. 16, no. 12, p. 4652, 2023.
[21] Y. Liu, G. Zhao, G. Li, W. He, and C. Zhong, "Analytical robust design optimization based on a hybrid surrogate model by combining polynomial chaos expansion and Gaussian kernel," *Structural and Multidisciplinary Optimization*, vol. 65, no. 11, p. 335, 2022.
[22] E. Denimal, L. Nechak, J. J. Sinou, and S. Nacivet, "A novel hybrid surrogate model and its application on a mechanical system subjected to friction-induced vibration," *Journal of Sound and Vibration*, vol. 434, pp. 456–474, 2018.
[23] Y. H. Li, M. M. Xiao, J. F. Shen, Y. Chao, L. Chen, and Z. Xin, "A dual objective global optimization algorithm based on adaptive weighted hybrid surrogate model for the hydrogen fuel utilization in hydrogen fuel cell vehicle," *International Journal of Hydrogen Energy*, vol. 48, no. 30, pp. 11390–11409, 2023.
[24] Z. Meng, Z. H. Zhang, H. L. Zhou, H. Chen, and B. Yu, "Robust design optimization of imperfect stiffened shells using an active learning method and a hybrid surrogate model," *Engineering Optimization*, vol. 52, no. 12, pp. 2044–2061, 2020.
[25] L. E. Zerpa, N. V. Queipo, S. Pintos, and J. L. Salager, "An optimization methodology of alkaline-surfactant-polymer flooding processes using field scale numerical simulation and multiple surrogates," *Journal of Petroleum Science and Engineering*, vol. 47, no. 3-4, pp. 197–208, 2005.
[26] T. Goel, R. T. Haftka, W. Shyy, and N. V. Queipo, "Ensemble of surrogates," *Structural and Multidisciplinary Optimization*, vol. 33, no. 3, pp. 199–216, 2007.
[27] J. Zhang, X. Yue, J. Qiu, M. Zhang, and X. Wang, "A unified ensemble of surrogates with global and local measures for global metamodelling," *Engineering Optimization*, vol. 53, no. 3, pp. 474–495, 2021.
[28] J. Q. Long, Y. Q. Liao, and P. Yu, "Multi-response weighted adaptive sampling approach based on hybrid surrogate model," *IEEE Access*, vol. 9, pp. 45441–45453, 2021.
[29] F. Ye, *Research on Optimization Design Method of Variable Stiffness Composite Materials Based on Proxy Model*, Hunan University, Changsha, China, 2021.
[30] Y. P. Hou, *Research on the Optimization Method for Layered Design and Discrete Structure Selection of Composite Laminates*, Dalian University of Technology, Dalian, China, 2013.
[31] N. Li, P. Chen, and Q. Ye, "A damage mechanics model for low-velocity impact damage analysis of composite laminates," *Aeronautical Journal*, vol. 121, no. 1238, pp. 515–532, 2017.
[32] J. B. Yang, *Optimization Design of Composite Laminated Structure with Variable Stiffness Layering Considering Process*, Northwest University of Technology, Xi'an, China, 2017.
[33] F. F. Wang, G. L. Yang, J. L. Ge, and F. J. Xu, "Lightweight design of a certain mortar base plate based on sensitivity analysis," *Journal of the Brazilian Society of Mechanical Sciences and Engineering*, vol. 43, no. 3, p. 126, 2021.
[34] Z. H. Zhang, Q. Ye, L. Fu, J. Q. Wang, M. Guo-Xiang, and Z. Q. Shen, "Rapid deformation calculation for large reflector antennas: a surrogate model method," *Research in Astronomy and Astrophysics*, vol. 23, no. 1, Article ID 015001, 2022.
[35] R. DeVlieg, K. Jeffries, and P. Vogeli, "High-speed fiber placement on large complex structures," in *Proceedings of the Aerospace Technology Conference and Exposition*, Orlando, FL, USA, September 2007.
[36] M. T. Emmerich, A. H. Deutz, and J. W. Klinkenberg, "Hypervolume-based expected improvement: monotonicity properties and exact computation," in *Proceedings of the Congress on Evolutionary Computation IEEE*, New Orleans, LA, USA, June 2011.
[37] M. Bai, X. Yan, and K. Wu, "Hybrid particle swarm algorithm for multiobjective optimization based on decomposition," *Computer Systems and Applications*, vol. 24, no. 12, pp. 215–222, 2015.
[38] Q. Zhang and H. Li, "MOEA/D: a multiobjective evolutionary algorithm based on decomposition," *IEEE Transactions on Evolutionary Computation*, vol. 11, no. 6, pp. 712–731, 2007.
[39] C. A. C. Coello, G. T. Pulido, and M. S. Lechuga, "Handling multiple objectives with particle swarm optimization," *IEEE*

*Transactions on Evolutionary Computation*, vol. 8, no. 3, pp. 256–279, 2004.

[40] A. W. Blom, C. S. Lopes, P. J. Kromwijk, Z. Gurdal, and P. P. Camanho, "A theoretical model to study the influence of tow-drop areas on the stiffness and strength of variable-stiffness laminates," *Journal of Composite Materials*, vol. 43, no. 5, pp. 403–425, 2009.

[41] M. J. Blondin and M. Hale, "An algorithm for multiobjective multi-agent optimization," in *Proceedings of the 2020 American Control Conference (ACC)*, Denver, CO, USA, July 2020.